View metadata, citation and similar papers at core.ac.uk
brought to you by CORE
provided by Scholarly Materials And Research @ Georgia Tech

Global optimization of sensitivity and dynamic range for two-center holographic recording

Omid Momtahan and Ali Adibi

School of Electrical and Computer Engineering, Georgia Institute of Technology, Atlanta, Georgia 30332-0001

Received June 19, 2002; revised manuscript received October 10, 2002

The performance of two-center holographic recording is theoretically studied and described in detail. We present a systematic method for global optimization of two-center holographic recording. Whereas the method presented is general, we perform optimization for lithium niobate crystals doped with iron and manganese ($LiNbO_3$:Fe:Mn). Both dynamic range ($M/\#$) and sensitivity (S) are considered for global optimization, and the optimum design parameters for $LiNbO_3$:Fe:Mn crystals are predicted. To achieve optimization we use both an analytic approach and a complete numerical approach. The absorption of light in the crystal is also considered. We show that the optimum design parameters for maximizing $M/\#$ are different from those for maximizing S. Therefore a trade-off exists between dynamic range and sensitivity. We also describe the complete dependence of S in two-center recording on the design parameters. We show in particular, for the first time to our knowledge, that S depends on the ratio of recording and sensitizing intensities and not on the absolute intensities. © 2003 Optical Society of America

OCIS codes: 090.0090, 090.2900, 210.2860, 160.2900, 050.7330.

1. INTRODUCTION

Holographic data storage is a promising technique for obtaining large-scale memory.[1–4] For this purpose the interference pattern of a signal (data) and a reference beam is recorded in a photorefractive crystal. Illuminating the crystal with the reference beam can retrieve the data. Among the photorefractive crystals, lithium niobate ($LiNbO_3$) has been most extensively investigated.[1,4–6] Conventional holographic recording experiments were performed in singly doped $LiNbO_3$ crystals, in particular in $LiNbO_3$:Fe (Refs. 1, 2, 4, and 6) and in $LiNbO_3$:Cu.[7,8] In these cases, readout resulted in the erasure of the stored information (destructive readout). Several methods, such as thermal fixing,[9,10] electrical fixing,[11,12] readout with wave-vector spectra,[13,14] two-step recording,[15–18] and two-center recording,[19,20] have been proposed for persistent holographic recording.

The two-center holographic recording method[19] proposed recently has attracted attention because of its ability to record persistent holograms. This method is based on use of two different dopants to provide shallower and deeper traps in photorefractive crystals.[19] The interference pattern of two lower-frequency (longer-wavelength) beams (reference and signal beams) is recorded in the presence of a higher-frequency (shorter-wavelength) beam (sensitizing beam). During the recording phase the sensitizing beam brings electrons from the deeper traps into the shallower traps via the conduction band, providing enough electron concentration in the shallower traps for holographic recording. The hologram will be recorded in both the shallower and the deeper traps. Readout is performed by the reference beam only. The readout by the reference beam partially erases the hologram by exciting electrons from the shallower traps. Eventually, all electrons in the shallower traps will be transferred to the deeper traps. The remaining hologram in the deeper traps will persist against further readout. The general recording and readout dynamics in two-center recording are shown in Fig. 1.

Three important performance measures in holographic storage are the dynamic range ($M/\#$; which is related to the available room for multiplexing different holograms), sensitivity or recording speed (S, which indicates how fast we can record a hologram with a fixed intensity and a fixed material thickness), and persistence (which indicates how many times we can read the stored information before data refreshing is required). The parameters that affect these measures in two-center recording are dopant concentrations, annealing (or oxidation–reduction), and recording and sensitizing intensities and wavelengths.

Several aspects of two-center recording were recently investigated.[20–32] Although most of the reported results were obtained for $LiNbO_3$:Fe:Mn crystals, other crystals such as $LiNbO_3$:Cu:Ce,[26] $LiNbO_3$:Tb:Fe,[28] and $LiNbO_3$:Ce:Mn (Ref. 29) were also investigated. However, there have been few efforts to optimize the method. Liu *et al.* presented the optimization for $M/\#$ in two-center recording with UV and red light and in $LiNbO_3$:Fe:Mn.[23,27] They considered the variation of only one parameter at a time. They used approximate formulas for the readout phase, and UV absorption was ignored in their analysis. The bulk photovoltaic effect of the Mn traps at the sensitizing wavelength was ignored. Also, the same recombination coefficient was used for electron recombination from the conduction band to either Mn or Fe traps. Adibi *et al.* optimized $LiNbO_3$:Fe:Mn, using UV and red beams for sensitizing and recording, respectively.[20] They used a reliable set of material parameters and considered the absorption of the sensitizing beam in their simulations. Using the numeric method supported by experimental results, they investigated the variation of $M/\#$ with only one parameter

0740-3224/2003/030449-13$15.00 © 2003 Optical Society of America

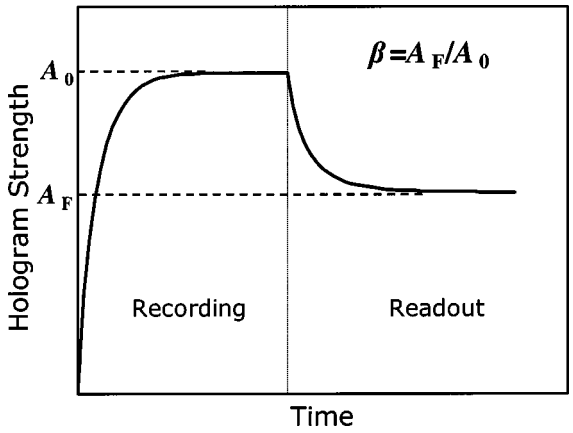

Fig. 1. Typical recording readout curve for two-center holographic recording. During the readout the hologram is partially erased. The remaining hologram persists against further readout.

at a time while all other parameters were fixed. In none of the previous efforts[20,23,27] considered here was the optimization of the sensitivity or its dependence on design parameters taken into account. Absorption of the recording beams was neglected in all the reports.

In this paper we describe the global optimization of both $M/\#$ and S for two-center recording. Accurate analytic formulas as well as complete numerical simulations are used. We also consider the absorption inside the crystal for both recording and sensitizing beams. A main feature of this study is that simultaneous variation of all design parameters is considered in the optimization process. Also, the variations of S with all design parameters are presented and explained for the first time to our knowledge. The theoretical limit of the performance for two-center recording in $LiNbO_3$:Fe:Mn is also presented.

In Section 2 we discuss the two-center model that we used for analysis of two-center recording. Performance measures are evaluated in Section 3. The procedure for optimization and also the effect of the different design parameters on $M/\#$ and S are discussed in Section 4. Optimum results are presented in Section 5. Conclusions are presented in Section 6.

2. TWO-CENTER MODEL

In general, two-center holographic recording can be described by Kukhtarev equations as modified for doubly doped crystals.[20,33] The system of nonlinear partial differential equations consists of two rate equations, for shallower and deeper traps; the current continuity equation; the current equation; and the Poisson equation for the space-charge field. These equations are

$$\frac{\partial N_D^-}{\partial t} = -(q_{D,L}s_{D,L}I_L + q_{D,H}s_{D,H}I_H)N_D^- + \gamma_D n(N_D - N_D^-), \quad (1)$$

$$\frac{\partial N_S^-}{\partial t} = -(q_{S,L}s_{S,L}I_L + q_{S,H}s_{S,H}I_H)N_S^- + \gamma_S n(N_S - N_S^-), \quad (2)$$

$$\frac{\partial j}{\partial x} = e\left(\frac{\partial N_D^-}{\partial t} + \frac{\partial N_S^-}{\partial t} + \frac{\partial n}{\partial t}\right), \quad (3)$$

$$j = e\mu nE + k_B T\mu\frac{\partial n}{\partial x} + (\kappa_{D,L}I_L + \kappa_{D,H}I_H)N_D^- + (\kappa_{S,L}I_L + \kappa_{S,H}I_H)N_S^-, \quad (4)$$

$$\frac{\partial E}{\partial x} = -\frac{e}{\varepsilon\varepsilon_0}(N_D^- + N_S^- + n - N_A), \quad (5)$$

with all variables and parameters as defined in Table 1. By assuming a sinusoidal variation of the recording intensity, i.e., that $I_L = I_{L0}[1 + m\cos(Kx)]$, and considering the first two terms in the spatial Fourier series of all variables, i.e., $N_D = N_{D0}^- + N_{D1}^-\exp(-iKx)$, we can find two sets of zeroth- and first-order equations as follows[20]:

$$\frac{dN_{D0}^-}{dt} = -(q_{D,L}s_{D,L}I_{L0} + q_{D,H}s_{D,H}I_H)N_{D0}^- + \gamma_D n_0(N_D - N_{D0}^-), \quad (6)$$

Table 1. Description of the Parameters Used in the Notation in This Paper[a]

Notation	Description
$q_{X,Y}s_{X,Y}$	Absorption cross section for absorbing a photon of beam Y and exciting an electron from trap X
$\kappa_{X,Y}$	Bulk photovoltaic coefficient of trap X at the wavelength of beam Y
$N_{X,l}^-$	Concentration of ionized dopant X
N_X	Total concentration of a dopant X
N_A	Concentration of positive compensator charge
n_l	Electron concentration
I_Y	Total intensity of beam Y
e	Electron charge
j_l	Current density
k_B	Boltzmann constant
γ_X	Recombination rate of the electrons to trap X
ρ	Total charge density
K	Magnitude of grating vector
μ	Electron mobility in the conduction band
m	Modulation depth
T	Crystal temperature
t	Time
$\varepsilon\varepsilon_0$	Primitivity of the crystal
λ_r	Recording wavelength
Θ	Half of the angle between the recording beams in the medium
n	Refractive index
r	Electro-optic coefficient
d	Crystal thickness

[a] l is an integer and can be 1 when it refers to first-order terms and 0 when it refers to zeroth-order terms. X and Y are variables and have the following subscripts: $X = S$, shallower traps; $X = D$, deeper traps; $Y = L$, lower-frequency (longer-wavelength) beam; $Y = H$, higher-frequency (shorter-wavelength) beam.

$$\frac{dN_{S0}^{-}}{dt} = -(q_{S,L}s_{S,L}I_{L0} + q_{S,H}s_{S,H}I_H)N_{S0}^{-} + \gamma_S n_0(N_S - N_{S0}^{-}), \quad (7)$$

$$0 = N_{D0}^{-} + N_{S0}^{-} + n_0 - N_A, \quad (8)$$

$$\frac{dN_{D1}^{-}}{dt} = -(q_{D,L}s_{D,L}I_{L0} + q_{D,H}s_{D,H}I_H)N_{D1}^{-} - q_{D,L}s_{D,L}mI_{L0}N_{D0}^{-} + \gamma_D n_1(N_D - N_{D0}^{-}) - \gamma_D n_0 N_{D1}^{-}, \quad (9)$$

$$\frac{dN_{S1}^{-}}{dt} = -(q_{S,L}s_{S,L}I_{L0} + q_{S,H}s_{S,H}I_H)N_{S1}^{-} - q_{S,L}s_{S,L}mI_{L0}N_{S0}^{-} + \gamma_S n_1(N_S - N_{S0}^{-}) - \gamma_S n_0 N_{S1}^{-}, \quad (10)$$

$$\frac{-iK}{e}j_1 = \left(\frac{dN_{D1}^{-}}{dt} + \frac{dN_{S1}^{-}}{dt} + \frac{dn_1}{dt}\right), \quad (11)$$

$$j_1 = e\mu n_0 E_1 - ik_B T\mu K n_1 + (\kappa_{D,L}I_{L0} + \kappa_{D,H}I_H)N_{D1}^{-} + \kappa_{D,L}mI_{L0}N_{D0}^{-} + (\kappa_{S,L}I_{L0} + \kappa_{S,H}I_H)N_{S1}^{-} + \kappa_{S,L}mI_{L0}N_{S0}^{-}, \quad (12)$$

$$\frac{iK}{e}E_1 = \frac{N_{D1}^{-} + N_{S1}^{-} + n_1}{\varepsilon\varepsilon_0}. \quad (13)$$

Note that in deriving these equations we replaced the derivative with respect to space variable ($\partial/\partial x$) with $-iK$. Further assumptions can simplify these equations. The variation of the electron concentration in the conduction band (n) is assumed to be instantaneous compared with the variation of the other variables (adiabatic approximation). We also assume that the electron concentration in the conduction band is negligible compared with the electron concentrations in the shallower and the deeper traps. The dc electric field (E_0) was also neglected in Eqs. (6)–(13).[20]

We should solve those eight equations simultaneously to find the space-charge field in the crystal. We then use the space-charge field to calculate hologram strength, $M/\#$, and S. The hologram strength is defined by $A = \pi n^3 r E_1 d/[2\lambda_r \cos(\Theta)]$; all the parameters are defined in Table 1. The relation between diffraction efficiency (η) and hologram strength is given by Kogelnik's formula[34] [i.e., $\eta = \sin^2(A)$].

3. DERIVATION OF THE PERFORMANCE MEASURES

In general, two-center holographic recording consists of three phases: sensitizing, recording, and readout. For a complete two-center recording process the crystal is first sensitized with the sensitizing beam. In the recording phase the hologram is recorded by the use of signal and reference beams (two coherent longer-wavelength beams), with the sensitizing beam (a shorter-wavelength beam) illuminating the crystal. During the readout phase the reference beam reads the hologram, and no other beam is present.

There are three measures that are used widely to describe the holographic recording process. The dynamic range, or $M/\#$, is a measure of the total refractive-index modulation that can be achieved for multiplexed holograms. If M holograms are multiplexed appropriately,[35] the diffraction efficiency of each hologram is $\eta = [(M/\#)/M]^2$. For recording weak holograms, an approximate measure for $M/\#$ is the square root of the saturation diffraction efficiency.[20] Sensitivity S is a measure of the speed of recording and is defined as

$$S = \frac{1}{I_L d} \times \left.\frac{d\sqrt{\eta}}{dt}\right|_{t=0}, \quad (14)$$

where I_L and d represent the total recording intensity and the crystal thickness, respectively. The persistence, or $R/\#$, is a measure of the number of times that a hologram can be read with acceptable diffraction efficiency.[36] During the readout in two-center recording, the hologram strength drops rapidly and then saturates at a nearly fixed value (Fig. 1). We refer to this value as the final hologram strength (A_F). The ratio of A_F to the saturation value of the hologram strength during recording (A_0) is denoted β in this paper. In the absence of an external electric field, $\beta \leqslant 0 \leqslant -1$.

The definition of common performance measures for normal (single-center) holographic recording should be slightly modified to describe the two-center holographic recording. For example, $M/\#$ and S calculated by use of recording dynamics should be multiplied by β for the two-center recording to account for partial erasure during readout.

A. Analytic Solution for the Recording Phase

In the recording phase we should solve differential equations (6)–(13) while the sensitizing and the recording intensities are not zero. $M/\#$ is proportional to the saturation space-charge field, and S is proportional to the slope of the space-charge field at the beginning of recording. Therefore, if we find a complete solution for the variation of the space-charge field with time, we can easily calculate $M/\#$ and S. We can find this solution by approximating the recording curve by a monoexponential function of time. Therefore the space-charge field is expressed by

$$E_1 \approx E_{SC}[1 - \exp(-t/\tau_r)], \quad (15)$$

where E_{SC} (saturation space-charge field during recording) and τ_r (recording time constant) are derived in Appendix A [relations (A1) and (A10), respectively]. Knowing E_{SC}, we can find $M/\#$:

$$M/\# = \frac{\pi n^3 r d}{2\lambda_r \cos(\Theta)} E_{SC}\beta, \quad (16)$$

where all the parameters are defined in Table 1. The value of β can be found from the analysis of readout phase (Subsection 3.B below). A typical recording curve for hologram strength obtained from the analytic formula for the space-charge field and the accurate curve that resulted from the numerical simulation for $LiNbO_3$:Fe:Mn

with a 365-nm sensitizing wavelength and a 633-nm recording wavelength are shown in Fig. 2. When the Fe concentration is much larger than the Mn concentration and the sensitizing intensity is 1 order of magnitude less than the recording intensities, the expressions for E_{SC} and τ_r can be simplified to relations (A13) and (A15), respectively (which we show here for clarity):

$$E_{SC} \approx \frac{\kappa_{Fe,R} N_{Fe0}^{-}}{e\mu n_0} m I_{R0} \times CF, \tag{A13}$$

$$\tau_r \approx \left(\frac{\varepsilon\varepsilon_0}{e\mu n_0}\right) + \left[\frac{\gamma_{Fe}(N_{Fe} - N_{Fe0}^{-}) + \gamma_{Mn}(N_{Mn} - N_{Mn0}^{-})}{H}\right]. \tag{A15}$$

The recording curve obtained from this approximation is also shown in Fig. 2. The expression for the saturation field (E_{CS}) is the same as the approximate expression for the saturation field in a normal holographic recording[6,37] in singly doped $LiNbO_3$, except that a correction factor (CF) is multiplied to include the effect of two-center recording. The recording time constant (τ_r) given in relation (A15) is the sum of the time constants for normal recording with an additional term that is due to two-center effects. Inasmuch as the additional term is always positive, we conclude that the time constant for two-center recording is always larger than that for normal recording under similar conditions.

A straightforward method for finding sensitivity S is to calculate the initial recording slope, using the approximate formula for the hologram strength as a function of time. But, as can be seen from Fig. 3, this is not a good approximation for the sensitivity in two-center recording. The reason is that the actual two-center recording dynamics is not optimally represented by a monoexponential function of time. Therefore we should use the initial differential equations and find the derivative of the space-charge field at the beginning of the recording ($t = 0$).

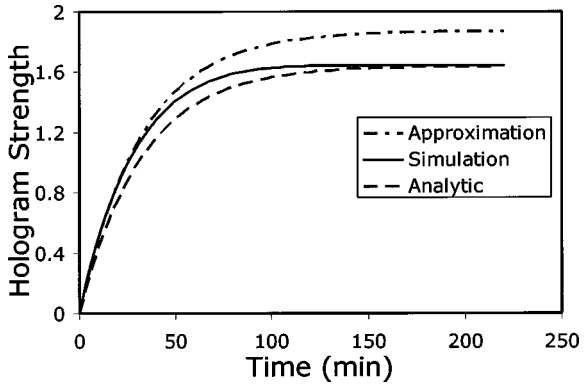

Fig. 2. Hologram strength versus time for a typical recording in a 1-mm-thick $LiNbO_3$ crystal doped with 0.15 wt. % Fe_2O_3 and 0.002 wt. % MnO by transmission geometry with $\Theta = 21.7°$. Initially, 80% of the Mn traps are filled with electrons. Sensitizing and recording intensities are 20 and 250 mW/cm^2, respectively. The absorption of both recording and sensitizing beams is neglected in this simulation. The polarization of the recording beams is ordinary.

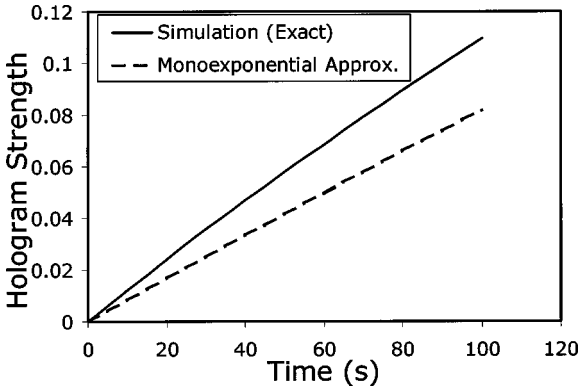

Fig. 3. Hologram strength at the beginning of recording used to show the difference between a monoexponential approximation and the accurate numerical solution. Sensitivity, by definition, is the initial slope of each curve. The parameters of recording are the same as those given in the caption of Fig. 2.

Finding the derivative with respect to time of both sides of Eq. (13), then using Eqs. (11) and (12) and also noting that N_{Fe1}^{-}, N_{Mn1}^{-}, n_1, and E_{sc} are zero at $t = 0$, we find that

$$S = \frac{1}{\varepsilon\varepsilon_0} \frac{\pi n^3 r}{2\lambda_r \cos(\Theta)} (\kappa_{D,L} N_{D0}^{-}|_{t=0} + \kappa_{S,L} N_{S0}^{-}|_{t=0}) m\beta, \tag{17}$$

where N_{D0}^{-} and N_{S0}^{-} are average electron concentrations in deeper and shallower traps, respectively (and are derived in Appendix A), and the other parameters are defined in Table 1. Again, β will be found in Subsection 3.B below. Note that N_{S0}^{-} and N_{D0}^{-} are at steady state when the sensitizing beam and the recording beams are present. The intensities of these beams must be equal to the average sensitizing and recording intensities, respectively, during the recording phase. In hologram multiplexing, each hologram (except the first hologram) is recorded after the material is illuminated long enough by sensitizing and recording beams (during the recording of previous holograms) to reach the steady-state values of N_{S0}^{-} and N_{D0}^{-}. In the definition of sensitivity in two-center recording, β is used to account for the partial erasure of the hologram at the beginning of readout. The sensitivity calculated from Eq. (17) agrees well with the numerical analysis. Inasmuch as the values of N_{D0}^{-} and N_{S0}^{-} are almost independent of the bulk photovoltaic coefficients of the shallower and the deeper traps, it can be seen that having dopants with higher photovoltaic constants results in higher sensitivity. This observation is exactly in accordance with the experimental results reported in Ref. 24. Considering the expressions for $M/\#$ and S [Eqs. (16) and (17)], we have all the analytic results for the recording phase.

B. Analysis of the Readout Phase

During readout, only the reference beam is present. The reference beam excites the electrons from the shallower traps to the conduction band. All electrons will eventually be retrapped in the deeper traps because the sensitizing beam is not present during readout and the reading beam cannot excite electrons from the deeper traps to the conduction band. Therefore the final persistent holo-

gram will be stored in the deeper traps. Finding an analytic solution for this phase is difficult because the average electron concentrations in the two traps (N_{D0}^- and N_{S0}^-) vary considerably with time. Numerical analysis for this phase shows that the intensity of the reference beam during readout has no effect on the final value of the space-charge field or on the hologram strength (Fig. 4). Note that modifying the dynamics of the readout intensity modifies the dynamics of the readout but that the final hologram strength (and, therefore, β) remains the same. Because the performance measures depend on β and not on the readout dynamics, we can choose an appropriate variation of the readout intensity with time to simplify the calculation of β (and other performance measures). The details of our method are summarized in Appendix B. The result is a second-order differential equation for the space-charge field:

$$P(W)\frac{d^2E_1}{dW^2} + Q(W)\frac{dE_1}{dW} + R(W)E_1 = 0, \qquad (18)$$

where

$$W = N_D - N_A + N_{S0}^-(t) \qquad (19)$$

and $P(W)$, $Q(W)$, and $R(W)$ are given in Appendix B for $LiNbO_3$:Fe:Mn crystals. The final value of the space-charge field is found by solution of Eq. (18) at $W = N_D - N_A$ (or $N_{S0}^- = 0$), which corresponds to the case for which all the shallower traps are empty. Although this equation must be solved numerically, it is much easier and faster to solve this equation rather than a set of five nonlinear differential equations that provides almost the same result for the final space-charge field. It is also easier to find the final value of E_1 ($E_{1,\mathrm{Final}}$) because this value is calculated at finite W ($W = N_D - N_A$) instead of at $t = \infty$; this reduces the computation time because the numerical solution at infinity is not needed. After finding the final value of the space-charge field we can calculate $\beta = E_{1,\mathrm{Final}}/E_{\mathrm{SC}}$, which will be used in finding the overall $M/\#$ and S [Eqs. (16) and (17)].

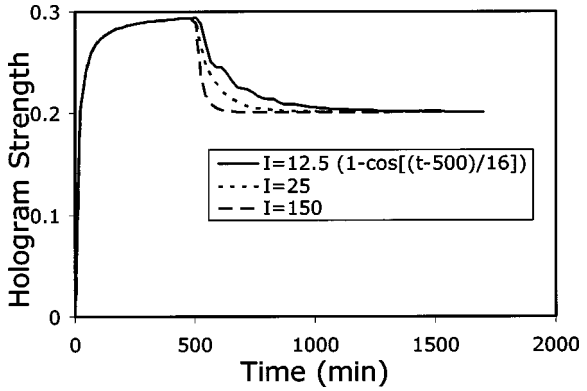

Fig. 4. Effect of readout intensity on hologram strength during the readout phase. The hologram is recorded in a 1-mm-thick $LiNbO_3$ crystal doped with 0.075 wt. % Fe_2O_3 and 0.01 wt. % MnO. Initially, 90% of the Mn traps are filled with electrons. Sensitizing and recording intensities are 20 and 500 mW/cm^2, respectively. The recording dynamics is the same in all cases. Readout intensities $I = 150$ mW/cm^2 and $I = 25$ mW/cm^2 are constant with time; for $I = 12.5(1 - \cos[(t - 500)/16])$ mW/cm^2, t represents time in minutes.

C. Effect of the Absorption of Sensitizing and Recording Beams

In most applications, the crystal used for two-center recording exhibits high absorption at the sensitizing wavelength. The absorption is stronger when the energy of the sensitizing photons is close to the energy bandgap of the crystal or when the total electron concentration in the traps is large. In such cases we should consider the absorption of the sensitizing beam as it goes through the crystal. Furthermore, when the electron concentration in the shallower traps becomes high during recording we should also consider the absorption of the recording beam inside the crystal. To include these absorptions in the calculation of $M/\#$ we first divide the crystal into several thin slices of thickness Δz (typically 50–100 slices for a 1-mm-thick crystal). Assuming constant sensitizing and recording intensities within each slice, we solve for $(M/\#)_i$ in each slice Δz. Then we calculate the total $M/\#$, using the following sum:

$$(M/\#)_{\mathrm{total}} = \sum_{\mathrm{all}\ i} (M/\#)_i . \qquad (20)$$

Equation (20) simply states that the total $M/\#$ of the crystal is the sum of the values $M/\#$ of the thin portions of the crystal with different sensitizing and recording beams. We also apply the idea of analyzing the thin slices to find the sensitivity when the absorption of both sensitizing and recording intensities is taken into account. Therefore the total sensitivity is found from

$$S_{\mathrm{total}} = \frac{\Delta z}{d}\sum_{\mathrm{all}\ i} S_i . \qquad (21)$$

4. OPTIMIZATION PROCEDURE

In this section we consider the role of each design parameter in the variation of $M/\#$ and S. In the simulations we use congruently melting $LiNbO_3$:Fe:Mn with different doping concentrations as the recording material. The sensitizing beam is a 365-nm UV beam with an intensity-absorption coefficient of the order of 9 mm^{-1}.[20] Two coherent recording beams with equal intensities are used at 633-nm (red) wavelength. We chose these wavelengths because a reliable set of all material parameters exists for $LiNbO_3$:Fe:Mn at 365 and 633 nm.[20] The hologram is recorded in a 1-mm-thick sample by use of symmetric transmission geometry. The angle between two recording beams is 43.5°. We assume ordinary polarization for recording and reading beams. The resultant grating vector is parallel to the c axis of the crystal.

Because finding the numerical solution for the readout phase is a time-consuming process, we consider the practical range for the design parameters and make a table of values of β for each set of parameters. Using the expressions found in Section 3 for the recording phase [i.e., Eqs. (16) and (17) and relation (A1) below] and also the complete table of β, we consider the behavior of the holographic measures as the design parameters vary. The variation of $M/\#$ with single design parameters (while other parameters are fixed at nonoptimal values) was reported previously.[20,23] Here we show the variation of

$M/\#$ with individual design parameters about its global optimum. We also explain these variations based on some simple approximate formulas. To the best of our knowledge, the variation of S with the design parameters about its global optimum is presented here for the first time.

To study the variation of $M/\#$ (or of S) with a single design parameter we fix all other design parameters at their global optimum values, which results in a global maximum for $M/\#$ (or for S). The details of the global optimization are presented in Section 5 below.

A. Role of Fe Concentration

In normal recording in a singly doped $LiNbO_3$ crystal, both $M/\#$ and S grow with increasing trap concentration. In two-center recording also, both $M/\#$ and S increase with increasing shallower trap concentration (Fe concentration). Figure 5 shows the variation of $M/\#$ and S with Fe concentration for a 1-mm-thick $LiNbO_3$:Fe:Mn crystal. Figure 5 shows that to achieve the maximum $M/\#$ and S we must use the highest possible Fe concentration. We know that the maximum value for Fe concentration in normal recording in $LiNbO_3$:Fe is $\sim$0.05 wt. %.[38] For higher Fe concentrations, electron tunneling between Fe traps prevents the recording of stronger holograms.[38] However, for two-center recording we choose the maximum concentration of 0.15 wt. % Fe_2O_3 ($N_{Fe} = 5 \times 10^{25}$ m^{-3}). In normal recording this concentration has the potential to show a tunneling effect, but in a doubly doped

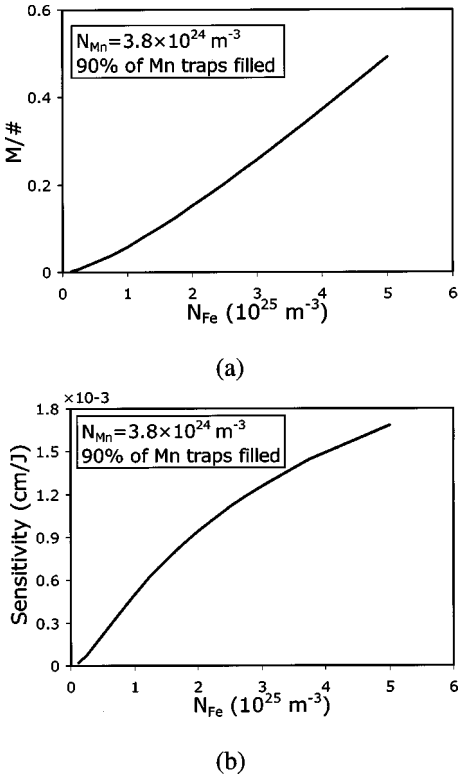

Fig. 5. Variation of (a) $M/\#$ and (b) S with Fe concentration in a 1-mm-thick $LiNbO_3$:Fe:Mn crystal. The Mn concentration is fixed at 3.8×10^{24} m^{-3}. Initially, 90% of the Mn traps are filled with electrons. The sensitizing and recording wavelengths are 365 nm (UV) and 633 nm (red), respectively. Intensity ratio (I_R/I_{UV}) is 25 for both cases.

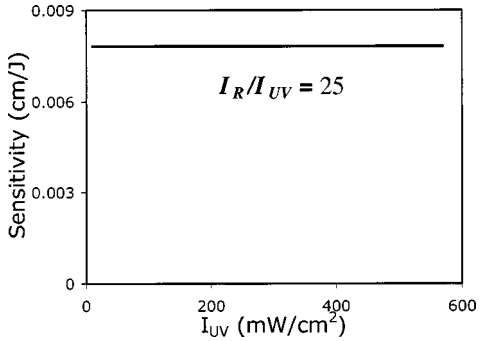

Fig. 6. Variation of S with sensitizing intensity for a 1-mm-thick $LiNbO_3$:Fe:Mn crystal doped with 0.075 wt. % Fe_2O_3 and 0.01 wt. % MnO. Initially, 90% of the Mn traps are filled with electrons. The sensitizing and recording wavelengths are 365 nm (UV) and 633 nm (red), respectively. The intensity ratio is fixed, and both the sensitizing and the recording intensities vary.

crystal we accept such a concentration for two reasons. First, the final hologram will be stored in the Mn traps, and all Fe traps will eventually be empty. Therefore, electron tunneling between Fe traps is not important. The second reason is that the tunneling between Fe traps during recording and readout tends to increase the hologram strength. The total space-charge field is due to two strong and almost 180° out-of-phase charge patterns in Fe and Mn traps.[20] Erasing one of the charge patterns by tunneling will result in increasing the total electric field. Such an increase in the space-charge field will increase the barrier against tunneling to prevent a further increase in the field. Therefore the Fe concentration is not limited by tunneling in two-center recording. Knowing that electron tunneling between Mn traps is harder than that between Fe traps,[39] we assume that $N_{Mn} = 3.7 \times 10^{25}$ m^{-3} (which corresponds approximately to 0.1 wt. % MnO) as the maximum practical Mn concentration.

B. Role of Sensitizing and Recording Intensities

Careful consideration of the expressions for $M/\#$ and S in the recording phase shows that both of them are functions of intensity ratio (I_R/I_{UV}) and not functions of absolute intensities [Eqs. (16) and (17)]. Also, noting that β is independent of the intensities yields that $M/\#$ and S for two-center recording depend only on the intensity ratio (I_R/I_{UV}) and not on the absolute intensities. The dependence of $M/\#$ on the intensity ratio was theoretically proposed and experimentally shown in Ref. 20, but we are aware of no previous report of the dependence of S on the intensity ratio. To our best knowledge, this is the first time that the dependence of S on the intensity ratio has been reported. Figure 6 shows this dependency more clearly. To explain this variation of S we can use the energy-band diagram in Fig. 7. S depends mainly on the bulk photovoltaic current density in the conduction band, which is proportional to the average electron concentration in the Fe traps (N_{Fe0}^-). This concentration depends on the excitation and recombination rates shown in Fig. 7. Excitation of the electrons from Fe traps tends to reduce N_{Fe0}^-, whereas excitation from the Mn traps tends to populate Fe traps (via the conduction band) and to increase N_{Fe0}^-. When we increase both intensities by the same factor (such that I_R/I_{UV} is fixed), all excitation rates

(proportional to light intensities) are increased in the same way. However, the relative strengths of these excitations remain intact. Thus the average electron concentrations in both Fe and Mn traps depend on the intensity ratio only and not on the absolute intensities. This intuitive point can be theoretically verified by Eqs. (A6) and (A7) derived in Appendix A.

The dependence of both $M/\#$ and S on the intensity ratio reduces one independent parameter (the design parameter is I_R/I_{UV} instead of both I_R and I_{UV}). With N_{Fe} already selected, three remaining parameters for optimization are Mn concentration (N_{Mn}), oxidization–reduction state (N_A), and intensity ratio (I_R/I_{UV}).

C. Role of Mn Concentration

Figure 8 shows the variation of $M/\#$ and S as the Mn concentration varies while the Fe concentration and the intensity ratio are fixed. For the calculation of $M/\#$ we assume that 85% of the Mn traps are initially filled with electrons because $M/\#$ reaches its global maximum when $N_A = 0.85\ N_{Mn}$. However, the maximum of S occurs when ~90% of the Mn traps are initially filled with electrons. As Fig. 8 shows, $M/\#$ reaches the global maximum when the Mn concentration is much lower than the Fe concentration and then decreases as the Mn concentration increases further. S, however, increases as the Mn concentration increases in the practical range of concentrations used for the simulations. The results shown in Fig. 8 can be understood by use of Eqs. (16) and (17).

With $N_{Mn} \approx 0$, no hologram can be recorded because all Fe traps are initially empty. Therefore, by increasing N_{Mn} we quickly increase the hologram strength (and $M/\#$). For small N_{Mn}, a space-charge limitation occurs and the approximate formulas are not useful. At larger values of N_{Mn} we can use relation (A13) for E_{SC} to substitute into Eq. (16) for $M/\#$. Therefore,

$$M/\# \propto \frac{N_{FeO^-}}{n_0}\,\mathrm{CF}, \tag{22}$$

where CF varies slowly with N_{Mn}. Increasing N_{Mn} results in increasing both N_{Fe0^-} and n_0. However, the increase in n_0 is stronger than that in N_{Fe0^-} for values of N_{Mn} above the optimal value. Therefore $M/\#$ decreases as N_{Mn} is increased. The actual positions of the peak depend strongly on the intensity ratio.

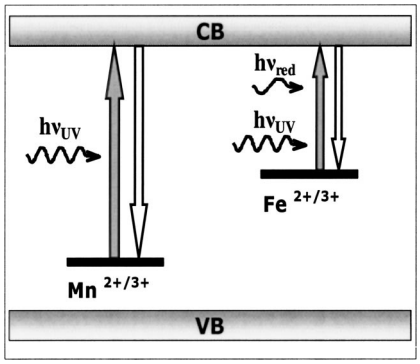

Fig. 7. Energy-band diagram for a typical $LiNbO_3$ crystal doped with Fe and Mn. CB and VB are conduction and valence bands, respectively.

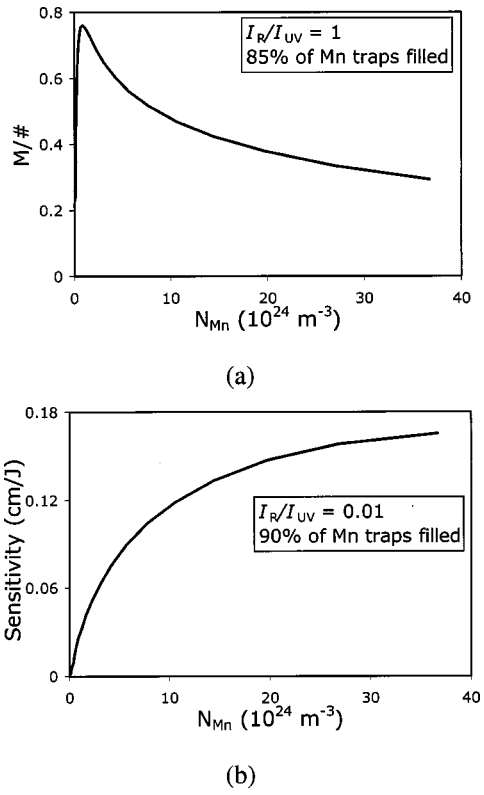

Fig. 8. Variation of (a) $M/\#$ and (b) S with Mn concentration for a 1-mm-thick $LiNbO_3$:Fe:Mn crystal doped with 0.15 wt.% Fe_2O_3. The sensitizing and recording wavelengths are 365 nm (UV) and 633 nm (red), respectively. For $M/\#$ in (a) the intensity ratio (I_R/I_{UV}) is 1, and initially 85% of the Mn traps are filled with electrons. For sensitivity in (b) the intensity ratio (I_R/I_{UV}) is 0.01 and initially 90% of the Mn traps are filled with electrons. These parameter values were selected to include the optimum $M/\#$ and S in the figures.

For sensitivity, because the photovoltaic constant of the Mn traps at the recording wavelength ($\kappa_{D,L}$) is negligible, we can assume that $S \propto N_{S0^-} = N_{Fe0^-}$. By increasing the Mn concentration (with 90% of the traps filled), we increase the excitation rate of electrons from the Mn traps to the conduction band (proportional to N_{Mn}). Increasing the concentration of the Mn traps will increase the recombination rate of electrons from the conduction band (proportional to N_{Mn}; note that 10% of the Mn traps are empty). The combination of these two competing effects results in variation of S with N_{Mn} as

$$S \propto N_{FeO^-} \propto \frac{N_{Mn}}{N_{Mn} + \xi}, \tag{23}$$

where ξ is a constant that represents the recombination rate for the Fe traps. The plot of relation (23) with N_{Mn} is the same as in Fig. 8(b).

It is obvious from Fig. 8 that the maximum values for $M/\#$ and S cannot be achieved simultaneously. Therefore there is a trade-off between $M/\#$ and S.

D. Role of Oxidization–Reduction State

The variations of $M/\#$ and S with the initial electron concentration in the Mn traps (i.e., N_A) are shown in Fig. 9; other parameters are fixed. The initial electron concen-

tration in Mn traps (N_A) can be varied by annealing (or oxidation–reduction). Figure 9 shows that both $M/\#$ and S reach their maximum values when $N_A \approx (0.8–0.9) \times N_{\mathrm{Mn}}$. The optimum values of N_A for maximizing $M/\#$ and S depend on the actual doping concentrations and on the intensity ratio. With $N_A = 0$, all traps (Mn and Fe) are empty, and no hologram can be recorded. With $N_A = N_{\mathrm{Mn}}$, all the Mn traps are initially filled with electrons. Although a strong hologram can be recorded in this case, the readout process is destructive (i.e., $\beta = 0$). All electrons will eventually be trapped in the Mn sites, with no empty Mn traps remaining to hold the final hologram.[21] Therefore there must be an optimum value of N_A at $0 < N_A < N_{\mathrm{Mn}}$ that results in maximum $M/\#$ or maximum S. The maxima for $M/\#$ and S usually do not occur at the same N_A, but the optimum values of N_A in the two cases are close.

E. Role of Intensity Ratio ($I_{\mathrm{R}}/I_{\mathrm{UV}}$)

For any crystal there is an optimum value for the intensity ratio ($I_{\mathrm{R}}/I_{\mathrm{UV}}$) that results in the best performance. Typical variations of $M/\#$ and S versus intensity ratio are shown in Fig. 10. Figure 10 shows that maximum S can be achieved with high sensitizing intensity, whereas the maximum $M/\#$ is obtained when the sensitizing and the recording intensities are of the same order. Note that

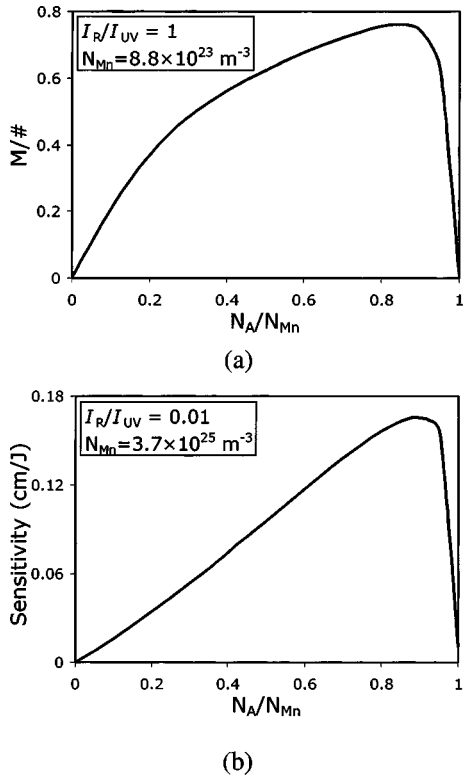

Fig. 9. Variation of (a) $M/\#$ and (b) S with initial oxidization–reduction state for a 1-mm-thick $LiNbO_3$:Fe:Mn crystal doped with 0.15 wt. % Fe_2O_3. The sensitizing and recording wavelengths, are 365 nm (UV) and 633 nm (red), respectively. For $M/\#$ in (a) the intensity ratio and the Mn concentration are 1 and 8.8×10^{23} m^{-3}, respectively. For sensitivity in (b) the intensity ratio and the Mn concentration are 0.01 and 3.7×10^{25} m^{-3}, respectively. The parameter values were chosen to include the optimum $M/\#$ and S in the figures.

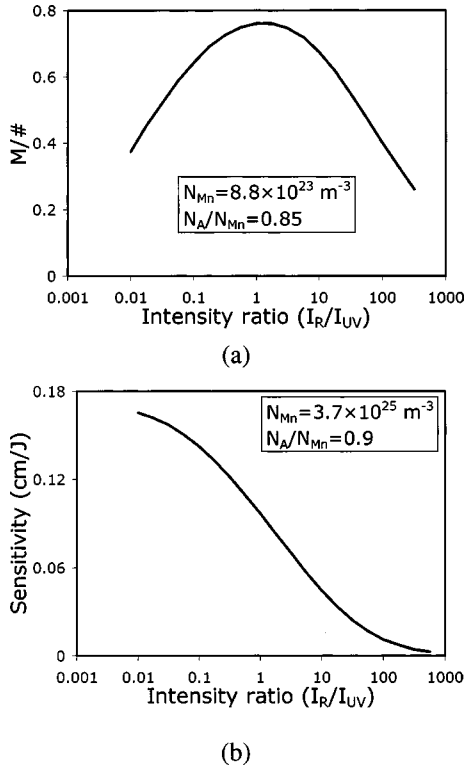

Fig. 10. Variation of (a) $M/\#$ and (b) S with intensity ratio for a 1-mm-thick $LiNbO_3$:Fe:Mn crystal doped with 0.15 wt. % Fe_2O_3. The sensitizing and recording wavelengths are 365 nm (UV) and 633 nm (red), respectively. For $M/\#$ in (a) the Mn concentration and the acceptor concentration (N_A) are 8.8×10^{23} and 7.5×10^{23} m^{-3}, respectively. For sensitivity in (b) the Mn concentration and the acceptor concentration are 3.7×10^{25} and 3.3×10^{25} m^{-3}, respectively. The parameter values are chosen to include the optimum $M/\#$ and S in the figures.

N_{Mn} and N_A/N_{Mn} in Fig. 10 are chosen to result in global optima. Therefore the global maxima of $M/\#$ and S occur at different values of the intensity ratio. The variation of $M/\#$ with intensity ratio, when other parameters are fixed at nonoptimal values, has already been reported and explained.[20,23] We can simply understand this variation by using relation (22). Both N_{Fe0^-} and n_0 depend on I_{R} and I_{UV}. Too strong a value of I_{UV} results in an acceptable N_{Fe0^-} (I_{UV} excites electrons from both Fe and Mn) and a strong n_0 ($n_0 \propto I_{\mathrm{UV}}$). Too weak a value of I_{UV} (compared to that of I_{R}) cannot populate the Fe traps because strong I_{R} tends to depopulate them. Therefore $M/\#$ is maximum at an intermediate $I_{\mathrm{R}}/I_{\mathrm{UV}}$. The actual optimum intensity ratio depends on N_{Fe}, N_{Mn}, and N_A. The variation of S with intensity ratio [Fig. 10(b)] reported here completely agrees with the experimental results of the variation of sensitivity with sensitizing and recording intensities reported in Ref. 40 for $LiNbO_3$:Cu:Ce crystals. It can easily be understood from Eq. (17) (i.e., $S \propto N_{\mathrm{Fe0}^-}$). The role of I_{UV} is to excite electrons from the Mn traps (and from the Fe traps). Its overall role is to populate the Fe traps to some degree. However, the role of I_{R} is only to depopulate the Fe traps. Therefore N_{Fe0^-} becomes larger at smaller $I_{\mathrm{R}}/I_{\mathrm{UV}}$, and larger N_{Fe0^-} results in larger S. So the maximum S is obtained at small $I_{\mathrm{R}}/I_{\mathrm{UV}}$ (or large $I_{\mathrm{UV}}/I_{\mathrm{R}}$).

5. GLOBAL OPTIMA

In Section 4 we observed the effect of the variation of the individual design parameters on $M/\#$ and S. The optimum obtained for each individual parameter (i.e., N_A) depends on the other design parameters. In general, the treatment of Section 4 cannot yield the set of parameters for the global maximum $M/\#$ (or maximum S). A global optimization scheme is required in which all design parameters are allowed to vary simultaneously.

In this optimization procedure we use the accurate analytic formulas that we derived for the recording phase [Eqs. (16) and (17) and relation (A1)] along with the table of β versus the design parameters calculated by numerical simulation of the readout phase. The absorption of sensitizing and recording beams is considered in our calculation, as explained in Subsection 3.C. We let all the parameters (N_{Mn}, N_A, and $I_{\mathrm{R}}/I_{\mathrm{UV}}$) vary and find the maximum $M/\#$ and S. The value of N_{Fe} is chosen at $N_{\mathrm{Fe}} = 5 \times 10^{25}\ \mathrm{m}^{-3}$, which corresponds to 0.15 wt. % Fe_2O_3.

In these simulations we used a 1-mm-thick $LiNbO_3$:Fe:Mn crystal. Sensitization and recording wavelengths were 365 and 633 nm, respectively. Ordinary polarization was used for recording and reading beams. We also calculated the optima for the more recently proposed set of wavelengths (404 nm for sensitization and 514 nm for recording).[24] For these wavelengths the set of material parameters can be estimated from the literature.[20,41,42] The estimated parameters that we used are summarized in Table 2.

Table 3 summarizes the optimum design parameters needed for maximizing $M/\#$ and S. It is obvious that S and $M/\#$ reach their maxima at different values of the design parameters, so there is always a trade-off in finding the best set of parameters.

For a sensitizing beam at 365 nm the crystal has a significant absorption coefficient, of the order of 9 mm^{-1}. Therefore, for a thick crystal, the intensity of the sensitizing beam drops dramatically as the beam passes through the crystal, and the intensity ratio deviates far from the optimum. If the absorption is decreased, a larger portion of the crystal will experience the intensity ratio close to the optimum value, and both $M/\#$ and S will increase. Therefore, using a longer sensitizing wavelength (which has lower absorption) can result in higher and $M/\#$. In addition, Fe traps are more sensitive 514- than to 633-nm wavelength; i.e., the bulk photovoltaic coefficient of the Fe traps is larger at 514 nm.[24] Therefore, recording at 514 nm results in higher $M/\#$ and S. The main disadvantage of using the 514-nm wavelength is that the reading beam can slightly excite electrons from Mn traps. Therefore a hologram recorded with recording beams at 514 nm will have a smaller value of $R/\#$.[24]

To our best knowledge, the maximum experimental values for $M/\#$ and S in a 1-mm-thick $LiNbO_3$:Fe:Mn crystal, with 365-nm sensitizing and 633-nm recording with ordinary polarization in transmission geometry, are 0.25/mm and 0.003 cm/J, respectively.[20] From Table 3 it can be seen that for 633- and 365-nm beams the maximum values of $M/\# = 0.76$/mm and $S = 0.17$ cm/J can be achieved by use of the optimum design parameters. By changing the recording and sensitizing beams to the new set at 514 and 404 nm we obtained further improvement. Note that by use of extraordinary polarization for recording beams both $M/\#$ and S can be further improved by a factor of 3 because of the larger electro-optic coefficient of $LiNbO_3$ for extraordinary polarization. Table 3 also represents the theoretical limit for $M/\#$ and S in $LiNbO_3$:Fe:Mn in accordance with material specification. These limits are $M/\# = 2.13$/mm and $S = 0.43$ cm/J, both obtained with sensitization at 404 nm and recording at 514 nm. With extraordinary polarization, $M/\# = 6.4$/mm and $S = 1.3$ cm/J can be obtained. One might obtain further improvements by application of a strong electric field[30] or by finding more-appropriate dopants.

As explained above, the strong trade-off between $M/\#$ and S must be considered in designing doubly doped crystals. For example, the maximum S is obtained when $I_{\mathrm{R}}/I_{\mathrm{UV}} = 0.01$, $N_{\mathrm{Mn}} = 3.7 \times 10^{25}$, and $N_A/N_{\mathrm{Mn}} = 0.9$.

Table 2. Crystal Parameters for $LiNbO_3$ at 514- and 404-nm Wavelengths

Notation	Description	Value
$q_{\mathrm{Fe},404}s_{\mathrm{Fe},404}$ (m^2/J)	Absorption cross section for absorbing a photon at wavelength 404 nm and exciting an electron from Fe traps to the conduction band	3.3×10^{-5}
$q_{\mathrm{Fe},514}s_{\mathrm{Fe},514}$ (m^2/J)	Absorption cross section for absorbing a photon at wavelength 514 nm and exciting an electron from Fe traps to the conduction band	1×10^{-5}
$q_{\mathrm{Mn},404}s_{\mathrm{Mn},404}$ (m^2/J)	Absorption cross section for absorbing a photon at wavelength 404 nm and exciting an electron from Mn traps to the conduction band	1.25×10^{-5}
$q_{\mathrm{Mn},514}s_{\mathrm{Mn},514}$ (m^2/J)	Absorption cross section for absorbing a photon at wavelength 514 nm and exciting an electron from Mn traps to the conduction band	1×10^{-8}
$-\kappa_{\mathrm{Fe},404}$ (m^3/V)	Bulk photovoltaic coefficient for Fe at 404 nm	13×10^{-33}
$-\kappa_{\mathrm{Fe},514}$ (m^3/V)	Bulk photovoltaic coefficient for Fe at 514 nm	3.8×10^{-33}
$-\kappa_{\mathrm{Mn},404}$ (m^3/V)	Bulk photovoltaic coefficient for Mn at 404 nm	2.9×10^{-33}
$-\kappa_{\mathrm{Mn},514}$ (m^3/V)	Bulk photovoltaic coefficient for Mn at 514 nm	5×10^{-36}
α (mm^{-1})	Absorption coefficient at 404 nm	≈ 1

Table 3. Optimum Design Parameters and Optimum $M/\#$ and S for $LiNbO_3$:Fe:Mn[a]

Measure	Recording Wavelength (nm)	Sensitizing Wavelength (nm)	N_{Mn} (m^{-3})	N_A (m^{-3})	I_R/I_{UV}	$M/\#$	S (cm/J)
Optimum for $M/\#$	633	365	8.8×10^{23}	7.5×10^{23}	1	0.76	0.016
	514	404	2.24×10^{24}	1.9×10^{24}	10	2.13	0.13
Optimum for S	633	365	3.7×10^{25}	3.3×10^{25}	0.01	0.17	0.17
	514	404	1.97×10^{25}	1.67×10^{25}	0.01	0.01	0.43

[a] The hologram is recorded in transmission geometry. The crystal thickness is 1 mm. The polarization of the recording beams is ordinary. Optimum N_{Fe} is 5×10^{25} m^{-3} in all cases.

For this set of parameters, $M/\#$ is low. The large I_{UV} compared to I_R does not allow strong holograms to build up. The optimum $M/\#$ is obtained when S is low. For practical applications in which low $M/\#$ or S is undesirable, the design parameters should be selected appropriately to result in the desired set of $M/\#$ and S.

6. CONCLUSIONS

We have presented a global optimization scheme for two-center holographic recording in doubly doped crystals. Our method is based on a combination of analytic formulas derived here with numerical simulations. We considered both dynamic range and sensitivity in our method. We found the global optimum set of design parameters by varying all parameters simultaneously. We implemented the method for $LiNbO_3$:Fe:Mn crystals and found the optimum set of parameters for maximizing dynamic range $M/\#$ and sensitivity S at different reading and sensitizing wavelengths.

Our results show that the best $M/\#$ and S that can be obtained in two-center recording in $LiNbO_3$:Fe:Mn crystals are 2.13/mm and 0.43 cm/J, respectively, when ordinary polarization is used. With extraordinary polarization for recording and reading beams, $M/\# = 6.4$/mm and $S = 1.3$ cm/J can be achieved. These results are obtained when sensitizing and recording wavelengths are 404 nm and 514 nm, respectively. The maximum of $M/\#$ can be achieved when N_{Fe} is as large as possible, when N_{Mn} is more than 1 order of magnitude smaller than N_{Fe}, when ~85% of Mn traps are initially filled, and when the recording and sensitizing intensities are of the same order. The optimum value of S, however, is obtained when both N_{Fe} and N_{Mn} are as large as possible, when ~90% of the Mn traps are initially occupied by electrons, and when the sensitizing intensity is ~100 times larger than the recording intensity. Note that the optimum set of parameters for maximizing $M/\#$ and S is different. The maximum values of $M/\#$ and S cannot be achieved simultaneously, and a trade-off exists.

We have also presented here, for the first time to our knowledge, the complete dependence of S on the various design parameters. We showed that S is a function of the ratio between recording and sensitizing intensities (I_R/I_{UV}) and not of the absolute intensities.

APPENDIX A

Considering the steady-state solutions of Eqs. (6)–(13) by setting all the time derivatives to zero and solving for E_1, we find that

$$E_{SC} = E_1|_{t\to\infty} \approx \frac{-1}{\varepsilon\varepsilon_0}\left[\frac{B_S\gamma_S(N_S - N_{S0}^-) + B_D\gamma_D(N_D - N_{D0}^-)}{C_S\gamma_S(N_S - N_{S0}^-) + C_D\gamma_D(N_D - N_{D0}^-)}\right]mI_{L0}, \quad \text{(A1)}$$

where the B and C coefficients are

$$B_S = (\kappa_{S,L}N_{S0}^- + \kappa_{D,L}N_{D0}^-)(q_{D,L}s_{D,L}I_{L0} + q_{D,H}s_{D,H}I_H + \gamma_D n_0) + q_{D,L}s_{D,L}N_{D0}^-[(\kappa_{S,L} - \kappa_{D,L})I_{L0} + (\kappa_{S,H} - \kappa_{D,H})I_H], \quad \text{(A2)}$$

$$B_D = (\kappa_{S,L}N_{S0}^- + \kappa_{D,L}N_{D0}^-)(q_{S,L}s_{S,L}I_{L0} + q_{S,H}s_{S,H}I_H + \gamma_S n_0) + q_{S,L}s_{S,L}N_{S0}^-[(\kappa_{D,L} - \kappa_{S,L})I_{L0} + (\kappa_{D,H} - \kappa_{S,H})I_H], \quad \text{(A3)}$$

$$C_S = \left[\frac{e\mu n_0}{\varepsilon\varepsilon_0} + \frac{iK}{e}(\kappa_{S,L}I_{L0} + \kappa_{S,H}I_H)\right](q_{D,L}s_{D,L}I_{L0} + q_{D,H}s_{D,H}I_H + \gamma_D n_0), \quad \text{(A4)}$$

$$C_D = \left[\frac{e\mu n_0}{\varepsilon\varepsilon_0} + \frac{iK}{e}(\kappa_{D,L}I_{L0} + \kappa_{D,H}I_H)\right](q_{S,L}s_{S,L}I_{L0} + q_{S,H}s_{S,H}I_H + \gamma_S n_0), \quad \text{(A5)}$$

the variables N_{S0}^-, N_{D0}^-, and n_0 are given by

$$N_{S0}^- = \frac{\{[\Gamma_D(N_D - N_A) - \Gamma_S(N_S - N_A)]^2 + 4\Gamma_D\Gamma_S N_D N_S\}^{1/2} - \Gamma_S(N_S + N_A) - \Gamma_D(N_D - N_A)}{2(\Gamma_D - \Gamma_S)}, \quad \text{(A6)}$$

$$N_{D0}^{-} = N_A - N_{S0}^{-}, \tag{A7}$$

$$n_0 = \frac{(\Gamma_D/\gamma_S)N_{S0}^{-} + (\Gamma_S/\gamma_D)N_{D0}^{-}}{\gamma_S(N_S - N_{S0}^{-}) + \gamma_D(N_D - N_{D0}^{-})}, \tag{A8}$$

and coefficients Γ_S and Γ_D are

$$\Gamma_S = \gamma_S(q_{D,L}s_{D,L}I_{L0} + q_{D,H}s_{D,H}I_H), \tag{A9a}$$

$$\Gamma_D = \gamma_D(q_{S,L}s_{S,L}I_{L0} + q_{S,H}s_{S,H}I_H). \tag{A9b}$$

All other variables and parameters are defined in Table 1.

To find the recording time constant, we should find the differential equation for the space-charge field. Because the space-charge field is proportional to $N_{S1}^{-} + N_{D1}^{-}$, by using Eqs. (9)–(12) and by appropriate substitutions we find a second-order linear differential equation with time-varying coefficients for the space-charge field. To find an approximate formula for recording a time constant we assume that the space-charge field can be represented by a monoexponential function of time. Assuming that the zeroth-order terms reach their steady-state values much faster than the first-order terms (we justify this assumption by using numerical simulations) results in a first-order differential equation with constant coefficient for $N_{S1}^{-} + N_{D1}^{-}$.

In this case the recording time constant can be written as

$$\tau_r \approx \frac{G_S\gamma_S(N_S - N_{S0}^{-}) + G_D\gamma_D(N_D - N_{D0}^{-})}{C_S\gamma_S(N_S - N_{S0}^{-}) + C_D\gamma_D(N_D - N_{D0}^{-})}, \tag{A10}$$

where C_S and C_D are given by Eqs. (A4) and (A5) and G_S and G_D are defined as

$$G_S = \left[\frac{e\mu n_0}{\varepsilon\varepsilon_0} + \frac{iK}{e}(\kappa_{S,L}I_{L0} + \kappa_{S,H}I_H)\right] + (q_{D,L}s_{D,L}I_{L0} + q_{D,H}s_{D,H}I_H + \gamma_D n_0), \tag{A11}$$

$$G_D = \left[\frac{e\mu n_0}{\varepsilon\varepsilon_0} + \frac{iK}{e}(\kappa_{D,L}I_{L0} + \kappa_{D,H}I_H)\right] + (q_{S,L}s_{S,L}I_{L0} + q_{S,H}s_{S,H}I_H + \gamma_S n_0). \tag{A12}$$

For the $LiNbO_3$ crystal doped with Fe and Mn and for recording with red and sensitizing with UV, relations (A1) and (A10) can be simplified further. When the sensitizing intensity is much lower than the recording intensity ($I_{UV} \ll I_R$) and the Mn concentration is much less than the Fe concentration, the following approximate formula can be obtained for the space-charge field:

$$E_{SC} = \frac{\kappa_{Fe,R}N_{Fe0}^{-}}{e\mu n_0} m I_{R0} \times \mathrm{CF}, \tag{A13}$$

where we can find all the parameters and variables from Table 1 by replacing the subscripts S with Fe, D with Mn, L with R, and H with UV. Similarly, N_{Fe0}^{-} can be found from Eq. (A6). Also, the factor CF is introduced as

$$\mathrm{CF} = \left[1 + \frac{q_{Fe,R}s_{Fe,R}I_{R0}\gamma_{Mn}(N_{Mn} - N_{Mn0}^{-})}{H}\right]^{-1}, \tag{A14}$$

where H is defined as

$$H = q_{Fe,UV}s_{Fe,UV}I_{UV}\gamma_{Mn}(N_{Mn} - N_{Mn0}^{-}) + q_{Mn,UV}s_{Mn,UV}I_{UV}\gamma_{Fe}(N_{Fe} - N_{Fe0}^{-}) + \gamma_{Fe}\gamma_{Mn}n_0(N_{Mn} + N_{Fe} - N_A).$$

For the same condition (i.e., $I_{UV} \ll I_R$ and $N_{Mn} \ll N_{Fe}$), the recording time constant is given approximately by

$$\tau_r \approx \left(\frac{\varepsilon\varepsilon_0}{e\mu n_0}\right) + \left[\frac{\gamma_{Fe}(N_{Fe} - N_{Fe0}^{-}) + \gamma_{Mn}(N_{Mn} - N_{Mn0}^{-})}{H}\right]. \tag{A15}$$

APPENDIX B

Finding the analytic solution for the readout phase is difficult. The main problem is that we cannot further assume that the average electron concentrations in the shallower and the deeper traps are constant. In this case we should solve all the zeroth- and first-order equations simultaneously, and a closed-form solution cannot be found easily. Because the most important part of the solution in this phase is the final value for the space-charge field, we concentrate on finding this value. During the readout process, the reading beam excites electrons from the shallower traps to the conduction band. These electrons will eventually be trapped and remain in the deeper traps. It is expected that varying the intensity of the reference beam will change only the dynamics of the process and will not affect the final electron concentrations in the deeper traps. Simulating the readout phase by reference beams with different intensities agrees well with this observation and shows that the final electron concentration in deeper traps (and, therefore, the final hologram strength) is independent of the intensity of the readout beam (Fig. 4). Using this fact, we can assume an appropriate variation of the reading beam intensity with time to simplify the equations. This intensity variation is given by

$$I_R(t) = I_0\left\{\frac{\gamma_{Fe}N_{Fe}}{\gamma_{Mn}[N_{Mn} - N_A + N_{Fe0}^{-}(t)]} + 1\right\}, \tag{B1}$$

where I_0 is a constant intensity and we can find all other variables and parameters from Table 1 by replacing the subscripts S with Fe and D with Mn. As we are interested in $LiNbO_3$:Fe:Mn crystals, we used the proper notation for this crystal in Eq. (B1). We further assume that $N_{Fe0}^{-} \ll N_{Fe}$. This assumption is acceptable because, for practical $LiNbO_3$:Fe:Mn crystals, N_A is much less than the Fe concentration. Also, the average electron concentration in the Fe traps (N_{Fe0}^{-}) continuously decreases with time during readout. Therefore, except at the early stage of readout, the assumption that $N_{Fe0}^{-} \ll N_{Fe}$ is valid.

Solving for N_{Fe0}^{-} from the zeroth-order equations results in

$$N_{Fe0}^{-}(t) = N_0 \exp(-q_{Fe,R}s_{Fe,R}I_0 t), \tag{B2}$$

where N_0 is the concentration of Fe^{2+} traps at the beginning of the readout, i.e., $N_0 = N_{Fe0}^{-}(t = 0)$, and $q_{Fe,R}s_{Fe,R}$ is the absorption cross section of red photons to excite electrons from Fe traps to the conduction band. Then we find N_{Mn0}^{-} and n_0 by using Eqs. (A7) and (A8) and substitute all the zeroth-order terms into the first-order equations. In the next step we change the variable from time (t) to $W = N_{Mn} - N_A + N_{Fe0}^{-}(t)$. The derivative with respect to time (i.e., d/dt) will be replaced by

$$\frac{d}{dt} = -q_{Fe,R}s_{Fe,R}I_0(W - N_{Mn} + N_A)\frac{d}{dW}.$$

Note that N_{Mn} and N_A are constant with time and that $W - N_{Mn} + N_A = N_{Fe0}^{-}(t)$ is given by Eq. (B2).

After some algebraic manipulations we reach the following differential equation for the space-charge field:

$$P(W)\frac{d^2E_1}{dW^2} + Q(W)\frac{dE_1}{dW} + R(W)E_1 = 0, \quad \text{(B3)}$$

where the coefficients are given by

$$P(W) = \gamma_{Mn}W^2(\gamma_{Mn}W^2 + [\gamma_{Fe}N_{Fe} + \gamma_{Mn}(N_A - N_{Mn})]W + \gamma_{Fe}N_{Fe}(N_A - N_{Mn})), \quad \text{(B4)}$$

$$Q(W) = -W\left(\gamma_{Mn}\left(\frac{e\mu}{\varepsilon\varepsilon_0} + \gamma_{Fe}\right)W^2 + \left\{\frac{e\mu}{\varepsilon\varepsilon_0}[\gamma_{Fe}N_{Fe} + \gamma_{Mn}(N_A - N_{Mn})] + \gamma_{Fe}\gamma_{Mn}(N_A - N_{Mn}) + \frac{iK\kappa_{Fe,R}}{eq_{Fe,R}s_{Fe,R}}\gamma_{Fe}\gamma_{Mn}N_{Fe}\right\}W + \left[\frac{e\mu}{\varepsilon\varepsilon_0}\gamma_{Fe}N_{Fe}(N_A - N_{Mn}) + \frac{iK\kappa_{Fe,R}}{eq_{Fe,R}s_{Fe,R}}\gamma_{Fe}{}^2N_{Fe}{}^2\right]\right), \quad \text{(B5)}$$

$$R(W) = \frac{e\mu}{\varepsilon\varepsilon_0}(\gamma_{Fe} + \gamma_{Mn})W^2 + \left\{\frac{e\mu}{\varepsilon\varepsilon_0}[\gamma_{Fe}N_{Fe} + (\gamma_{Fe} + \gamma_{Mn})(N_A - N_{Mn})] + \frac{iK\kappa_{Fe,R}}{eq_{Fe,R}s_{Fe,R}}\gamma_{Fe}\gamma_{Mn}N_{Fe}\right\}W + \left[\frac{e\mu}{\varepsilon\varepsilon_0}\gamma_{Fe}N_{Fe}(N_A - N_{Mn}) + \frac{iK\kappa_{Fe,R}}{eq_{Fe,R}s_{Fe,R}}\gamma_{Fe}{}^2N_{Fe}{}^2\right], \quad \text{(B6)}$$

and we can find all the parameters from Table 1 by replacing the subscripts S with Fe, D with Mn, and L with R. To find the final space-charge field (after sufficient readout) we should solve differential equation (B3) and find the solution at $W = N_{Mn} - N_A$. The initial conditions at $t = 0$, $W(t = 0) = W_0 = N_{Mn} - N_A + N_0$, are

$$E_1(W_0) = E_1(t = 0) = E_{SC}, \quad \text{(B7)}$$

$$\left.\frac{dE_1}{dW}\right|_{W=W_0} = \left(\frac{e}{\varepsilon\varepsilon_0}\right)^2\frac{\mu}{iK}\frac{1}{\gamma_{Mn}W_0} + \frac{\kappa_{Fe,R}}{\varepsilon\varepsilon_0 q_{Fe,R}s_{Fe,R}}\frac{1}{N_0} \times \left(1 + \frac{\gamma_{Fe}N_{Fe}}{\gamma_{Mn}W_0}\right)N_{Fe1}{}^{-}(t = 0), \quad \text{(B8)}$$

where E_{sc} and $N_{Fe1}{}^{-}(t = 0)$ are the saturation space-charge field and the first-order electron concentration in Fe traps, respectively, at the beginning of the readout. Both E_{sc} and $N_{Fe1}{}^{-}(t = 0)$ are calculated from the analytic solution of the recording phase.

ACKNOWLEDGMENT

This study was supported by the Yamacraw Research Program, a State of Georgia initiative in broadband communications design, and by the U.S. Air Force Office of Scientific Research (G. Pomrenke) under agreement F49620-02-1-0053.

A. Adibi's e-mail address is adibi@ece.gatech.edu.

REFERENCES

1. F. H. Mok, "Angle-multiplexed storage of 5000 holograms in lithium niobate," Opt. Lett. **18**, 915–917 (1993).
2. J. F. Heanue, M. C. Bashaw and L. Hesselink, "Volume holographic storage and retrieval of digital data," Science **265**, 749–752 (1994).
3. D. Psaltis and F. Mok, "Holographic memories," Sci. Am. **273**, 70–76 (1995).
4. D. Psaltis and G. W. Burr, "Holographic data storage," IEEE Comput. **31**(2), 52–60 (1998).
5. D. L. Staebler and J. J. Amodei, "Coupled-wave analysis of holographic storage in $LiNbO_3$," J. Appl. Phys. **43**, 1042–1049 (1972).
6. A. Yariv, S. S. Orlov, and G. A. Rakuljic, "Holographic storage dynamics in lithium niobate: theory and experiment," J. Opt. Soc. Am. B **13**, 2513–2523 (1996).
7. O. Mikami, "Cu-diffused layers in $LiNbO_3$ for reversible holographic storage," Opt. Commun. **11**, 30–32 (1975).
8. P. Hertel, K. H. Ringhofer, and R. Sommerfeldt, "Theory of thermal hologram fixing and application to $LiNbO_3$:Cu," Phys. Status Solidi A **104**, 855–862 (1987).
9. J. J. Amodei and D. L. Staebler, "Holographic pattern fixing in electro-optic crystals," Appl. Phys. Lett. **18**, 540–542 (1971).
10. X. An, D. Psaltis, and G. W. Burr, "Thermal fixing of 10,000 holograms in $LiNbO_3$:Fe," Appl. Opt. **38**, 386–393 (1999).
11. F. Micheron and G. Bismuth, "Electrical control of fixing and erasure of holographic pattern in ferroelectric materials," Appl. Phys. Lett. **20**, 79–81 (1972).
12. J. A. Ma, T. Chang, J. Hong, R. Neurgaonkar, G. Barbastathis, and D. Psaltis, "Electrical fixing of 1000 angle-multiplexed holograms in SBN:75," Opt. Lett. **22**, 1116–1118 (1997).
13. H. C. Kulich, "A new approach to read volume holograms at different wavelengths," Opt. Commun. **64**, 407–411 (1987).
14. E. Chuang and D. Psaltis, "Storage of 1000 holograms with use of a dual-wavelength method," Appl. Opt. **36**, 8445–8454 (1997).
15. D. von der Linde, A. M. Glass, and K. F. Rodgers, "Multiphoton photorefractive process for optical storage in $LiNbO_3$" Appl. Phys. Lett. **25**, 155–157 (1974).
16. K. Buse, F. Jermann, and E. Krätzig, "Two-step photorefractive hologram recording in $LiNbO_3$:Fe," Ferroelectrics **141**, 197–205 (1993).
17. L. Hesselink, S. S. Orlov, A. Liu, A. Akella, D. Lande, and R. R. Neurgaonkar, "Photorefractive materials for nonvolatile volume holographic data storage," Science **282**, 1089–1094 (1998).
18. H. Guenther, R. Macfarlane, Y. Furukawa, K. Kitamura, and R. Neurgaonkar, "Two-color holography in reduced near-stoichiometric lithium niobate," Appl. Opt. **37**, 7611–7623 (1998).
19. K. Buse, A. Adibi, and D. Psaltis, "Non-volatile holographic recording in doubly doped lithium niobate crystals," Nature **393**, 665–668 (1998).

20. A. Adibi, K. Buse, and D. Psaltis, "Two-center holographic recording," J. Opt. Soc. Am. B **18**, 584–601 (2001).
21. A. Adibi, K. Buse, and D. Psaltis, "Effect of annealing in two-center holographic recording," Appl. Phys. Lett. **74**, 3767–3769 (1999).
22. C. Moser, B. Schupp, and D. Psaltis, "Localized holographic recording in doubly doped lithium niobate," Opt. Lett. **25**, 162–164 (2000).
23. Y. Liu, L. Liu, and C. Zhou, "Prescription for optimizing holograms in $LiNbO_3$:Fe:Mn," Opt. Lett. **25**, 551–553 (2000).
24. A. Adibi, K. Buse, and D. Psaltis, "Sensitivity improvement in two-center holographic recording," Opt. Lett. **25**, 539–541 (2000).
25. Y. W. Liu, L. R. Liu, Y. C. Guo, and C. H. Zhou, "The dynamics of holographic storage in doubly doped $LiNbO_3$:Fe:Mn," Acta Phys. Sin. **49**, 880–886 (2000).
26. Y. W. Liu, L. R. Liu, C. H. Zhou, and L. Y. Xu, "Nonvolatile photorefractive holograms in $LiNbO_3$:Cu:Ce crystals," Opt. Lett. **25**, 908–910 (2000).
27. Y. W. Liu, L. R. Liu, C. H. Zhou, and L. Xu, "Photorefractive holographic dynamics in doubly doped $LiNbO_3$:Fe:Mn," Chin. Phys. Lett. **17**, 571–573 (2000).
28. M. Lee, S. Takekawa, Y. Furukawa, K. Kitamura, H. Hatano, and S. Tao, "Angle-multiplexed hologram storage in $LiNbO_3$:Tb, Fe," Opt. Lett. **25**, 1337–1339 (2000).
29. I. G. Kim, M. Lee, S. Takekawa, Y. Furukawa, K. Kitamura, L. Galambos, and L. Hesselink, "Volume holographic storage in near-stoichiometric $LiNbO_3$:Ce:Mn," Jpn. J. Appl. Phys., Part 2 **39**, L1094–L1069 (2000).
30. R. Fujimura, S. Ashihara, O. Matoba, T. Shimura, and K. Kuroda, "Enhancement of nonvolatile recording by an external field in doubly doped lithium niobate," in *Photorefractive Effects, Materials, and Devices*, Vol. 62 of OSA Trends in Optics and Photonics Series (Optical Society of America, Washington, D.C., 2001), pp. 212–216.
31. A. Adibi, K. Buse, and D. Psaltis, "The role of carrier mobility in holographic recording in $LiNbO_3$," Appl. Phys. B **72**, 653–659 (2001).
32. D. Liu, L. R. Liu, C. H. Zhou, J. Zhang, and L. Y. Xu, "Experimental study of accumulative recording during nonvolatile holographic storage in $LiNbO_3$:Fe:Mn crystals," Microwave Opt. Technol. Lett. **32**, 423–425 (2002).
33. F. Jermann and J. Otten, "Light-induced charge transport in $LiNbO_3$:Fe at high light intensities," J. Opt. Soc. Am. B **10**, 2085–2092 (1993).
34. H. Kogelnik, "Coupled wave theory for thick hologram grating," Bell Syst. Tech. J. **48**, 2909–2947 (1969).
35. D. Psaltis, D. Brady, and K. Wagner, "Adaptive optical network using photorefractive crystals," Appl. Opt. **27**, 1752–1759 (1988).
36. A. Adibi, K. Buse, and D. Psaltis, "System measure for persistence in holographic recording and application to singly doped and doubly doped lithium niobate," Appl. Opt. **40**, 5175–5182 (2001).
37. C. Gu, J. Hong, H. Li, D. Psaltis, and P. Yeh, "Dynamics of grating formation in photovoltaic media," J. Appl. Phys. **69**, 1167–1172 (1991).
38. I. Nee, M. Müller, K. Buse, and E. Krätzig, "Role of iron in lithium-niobate crystals for the dark-storage time of holograms," J. Appl. Phys. **88**, 4282–4286 (2000).
39. Y. P. Yang, K. Buse, and D. Psaltis, "Photorefractive recording in $LiNbO_3$:Mn," Opt. Lett. **27**, 158–160 (2002).
40. Y. W. Liu, L. R. Liu, D. A. Liu, L. Y. Xu, C. H. Zhou, "Intensity dependence of two-center nonvolatile holographic recording in $LiNbO_3$:Cu:Ce crystals," Opt. Commun. **190**, 339–343 (2001).
41. E. Kratzig and H. Kurz, "Photo-induced currents and voltages in $LiNbO_3$," Ferroelectrics **13**, 295–296 (1976).
42. E. Kratzig and H. Kurz, "Photorefractive and photovoltaic effects in doped $LiNbO_3$," Opt. Acta **24**, 475–482 (1977).